Two-shot fringe pattern phase-amplitude demodulation using Gram-Schmidt orthonormalization with Hilbert-Huang pre-filtering

Maciej Trusiak,[1,*] and Krzysztof Patorski[1]

[1]*Warsaw University of Technology, Institute of Micromechanics and Photonics,8 Sw. A. Boboli St., 02-525 Warsaw, Poland*

[*]*maciek.trusiak@gmail.com*

Abstract: Gram-Schmidt orthonormalization is a very fast and efficient method for the fringe pattern phase demodulation. It requires only two arbitrarily phase-shifted frames. Images are treated as vectors and upon orthogonal projection of one fringe vector onto another the quadrature fringe pattern pair is obtained. Orthonormalization process is very susceptible, however, to noise, uneven background and amplitude modulation fluctuations. The Hilbert-Huang transform based preprocessing is proposed to enhance fringe pattern phase demodulation by filtering out the spurious noise and background illumination and performing fringe normalization. The Gram-Schmidt orthonormalization process error analysis is provided and its filtering-expanded capabilities are corroborated analyzing DSPI fringes and performing amplitude demodulation of Bessel fringes. Synthetic and experimental fringe pattern analyses presented to validate the proposed technique show that it compares favorably with other pre-filtering schemes, i.e., Gaussian filtering and continuous wavelet transform.

OCIS codes: (100.2650) Fringe analysis; (110.2650) Fringe analysis; (120.2650) Fringe analysis; (120.3180) Interferometry; (120.5050) Phase measurement; (120.6160) Speckle interferometry.

References and links

1. J. Schwider, "Advanced evaluation techniques in interferometry," in *Progress in Optics,* E. Wolf ed. (Elsevier, 1990).
2. D. W. Robinson and G. Reid, *Interferogram Analysis: Digital Fringe Pattern Measurement* (Institute of Physics Publishing, 1993).
3. D. Malacara, M. Servin, and Z. Malacara, *Interferogram Analysis for Optical Testing* (Marcel Dekker, 1998).
4. D. Malacara, ed., *Optical Shop Testing* (Jon Wiley & Sons, 2007).
5. M. Takeda, H. Ina, and S. Kobayashi, "Fourier-transform method of fringe-pattern analysis for computer-based topography and interferometry," J. Opt. Soc. Am. **72**(1), 156–160 (1982).
6. D. J. Bone, H.-A. Bachor, and R. J. Sandeman, "Fringe-pattern analysis using a 2-D Fourier transform," Appl. Opt. **25**(10), 1653–1660 (1986).
7. J. H. Massig and J. Heppner, "Fringe-pattern analysis with high accuracy by use of the Fourier-transform method: theory and experimental tests," Appl. Opt. **40**(13), 2081–2088 (2001).
8. Q. Kemao, "Windowed Fourier transform for fringe pattern analysis," Appl. Opt. **43**(13), 2695–2702 (2004).
9. Q. Kemao, "Two-dimensional windowed Fourier transform for fringe pattern analysis: Principles, applications and implementations," Opt. Lasers Eng. **45**(2), 304–317 (2007).
10. Q. Kemao, H. Wang, and W. Gao, "Windowed Fourier transform for fringe pattern analysis: theoretical analyses," Appl. Opt. **47**(29), 5408–5419 (2008).
11. L. R. Watkins, S. M. Tan, and T. H. Barnes, "Determination of interferometer phase distributions by use of wavelets," Opt. Lett. **24**(13), 905–907 (1999).
12. K. Pokorski and K. Patorski, "Visualization of additive-type moiré and time-average fringe patterns using the continuous wavelet transform," Appl. Opt. **49**(19), 3640–3651 (2010).

#229019 - $15.00 USD Received 8 Dec 2014; revised 26 Jan 2015; accepted 26 Jan 2015; published 13 Feb 2015

13. K. Pokorski and K. Patorski, "Processing and phase analysis of fringe patterns with contrast reversals," Opt. Express **21**(19), 22596–22609 (2013).
14. M. Servin, J. L. Marroquin, and F. J. Cuevas, "Demodulation of a single interferogram by use of a two-dimensional regularized phase-tracking technique," Appl. Opt. **36**(19), 4540–4548 (1997).
15. M. Servin, J. L. Marroquin, and F. J. Cuevas, "Fringe-follower regularized phase tracker for demodulation of closed-fringe interferograms," J. Opt. Soc. Am. A **18**(3), 689–695 (2001).
16. L. Kai and Q. Kemao, "Improved generalized regularized phase tracker for demodulation of a single fringe pattern," Opt. Express **21**(20), 24385–24397 (2013).
17. M. Kujawinska and J. Wojciak, "Spatial-carrier phase-shifting technique of fringe pattern analysis," Proc. SPIE **1508**, 61–67 (1991).
18. M. Pirga and M. Kujawinska, "Two directional spatial-carrier phase-shifting method for analysis of crossed and closed fringe patterns," Opt. Eng. **34**(8), 2459–2466 (1995).
19. K. Creath and J. Schmit, "N-point spatial phase-measurement techniques for non-destructive testing," Opt. Lasers Eng. **24**(5–6), 365–379 (1996).
20. A. Styk, and K. Patorski, "Analysis of systematic errors in spatial carrier phase shifting applied to interferogram intensity modulation determination," Appl. Opt. **46**(21), 4613–46–24 (2007).
21. S. K. Debnath and Y.-K. Park, "Real-time quantitative phase imaging with a spatial phase-shifting algorithm," Opt. Lett. **36**(23), 4677–4679 (2011).
22. Y. Du, G. Feng, H. Li, J. Vargas, and S. Zhou, "Spatial carrier phase-shifting algorithm based on principal component analysis method," Opt. Express **20**(15), 16471–16479 (2012).
23. X. Zhu, Z. Chen, and C. Tang, "Variational image decomposition for automatic background and noise removal of fringe patterns," Opt. Lett. **38**(3), 275–277 (2013).
24. X. Zhu, C. Tang, B. Li, C. Sun, and L. Wang, "Phase retrieval for single frame projection fringe pattern with variational image decomposition," Opt. Lasers Eng. **59**(8), 25–33 (2014).
25. K. Patorski, K. Pokorski, and M. Trusiak, "Fourier domain interpretation of real and pseudo-moiré phenomena," Opt. Express **19**(27), 26065–26078 (2011).
26. M. Trusiak and K. Patorski, "Space domain interpretation of incoherent moiré superimpositions using FABEMD," Proc. SPIE **8697**, 869704 (2012).
27. M. Trusiak, K. Patorski, and M. Wielgus, "Adaptive enhancement of optical fringe patterns by selective reconstruction using FABEMD algorithm and Hilbert spiral transform," Opt. Express **20**(21), 23463–23479 (2012).
28. M. Trusiak, K. Patorski, and K. Pokorski, "Hilbert-Huang processing for single-exposure two-dimensional grating interferometry," Opt. Express **21**(23), 28359–28379 (2013).
29. M. Trusiak, M. Wielgus, and K. Patorski, "Advanced processing of optical fringe patterns by automated selective reconstruction and enhanced fast empirical mode decomposition," Opt. Lasers Eng. **52**(1), 230–240 (2014).
30. K. Patorski, M. Trusiak, and M. Wielgus, "Fast adaptive processing of low quality fringe patterns by automated selective reconstruction and enhanced fast empirical mode decomposition," Fringe **2013**, 185–190 (2014).
31. M. Trusiak, K. Patorski, and M. Wielgus, "Hilbert-Huang processing and analysis of complex fringe patterns," Proc. SPIE **9203**, 92030K (2014).
32. J. A. Guerrero, J. L. Marroquin, M. Rivera, and J. A. Quiroga, "Adaptive monogenic filtering and normalization of ESPI fringe patterns," Opt. Lett. **30**(22), 3018–3020 (2005).
33. T. M. Kreis and W. P. O. Jueptner, "Fourier transform evaluation of interference patterns: demodulation and sign ambiguity," Proc. SPIE **1553**, 263–273 (1992).
34. J. Vargas, J. A. Quiroga, T. Belenguer, M. Servín, and J. C. Estrada, "Two-step self-tuning phase-shifting interferometry," Opt. Express **19**(2), 638–648 (2011).
35. J. Vargas, J. A. Quiroga, C. O. S. Sorzano, J. C. Estrada, and J. M. Carazo, "Two-step interferometry by a regularized optical flow algorithm," Opt. Lett. **36**(17), 3485–3487 (2011).
36. J. Vargas, J. A. Quiroga, C. O. S. Sorzano, J. C. Estrada, and J. M. Carazo, "Two-step demodulation based on the Gram-Schmidt orthonormalization method," Opt. Lett. **37**(3), 443–445 (2012).
37. R. C. Gonzalez and R. E. Woods, *Digital Image Processing*, 2nd ed. (Prentice Hall, 2002).
38. J. A. Quiroga, J. A. Gomez-Pedrero, and A. Garcia-Botella, "Algorithm for fringe pattern normalization," Opt. Commun. **197**(1–3), 43–51 (2001).
39. N. A. Ochoa and A. A. Silva-Moreno, "Normalization and noise reduction algorithm for fringe patterns," Opt. Commun. **270**(2), 161–168 (2007).
40. K. Pokorski and K. Patorski, "Separation of complex fringe patterns using two-dimensional continuous wavelet transform," Appl. Opt. **51**(35), 8433–8439 (2012).
41. J. Ma, Z. Wang, and T. Pan, "Two-dimensional continuous wavelet transform algorithm for phase extraction of two-step arbitrarily phase-shifted interferograms," Opt. Lasers Eng. **55**(4), 205–211 (2014).
42. N. E. Huang, Z. Shen, S. R. Long, M. C. Wu, H. H. Shih, Q. Zheng, N. C. Yen, C. C. Tung, and H. H. Liu, "The empirical mode decomposition and the Hilbert spectrum for non-linear and non-stationary time series analysis," Proc. R. Soc. Lond. A **454**(1971), 903–995 (1998).
43. S. M. A. Bhuiyan, R. R. Adhami, and J. F. Khan, "Fast and adaptive bidimensional empirical mode decomposition using order-statistics filter based envelope estimation," EURASIP J. Adv. Signal Process. **164**, 725356 (2008).

#229019 - $15.00 USD Received 8 Dec 2014; revised 26 Jan 2015; accepted 26 Jan 2015; published 13 Feb 2015

44. K. G. Larkin, D. J. Bone, and M. A. Oldfield, "Natural demodulation of two-dimensional fringe patterns. I. General background of the spiral phase quadrature transform," J. Opt. Soc. Am. A **18**(8), 1862–1870 (2001).
45. K. G. Larkin, D. J. Bone, and M. A. Oldfield, "Natural demodulation of two-dimensional fringe patterns. II. Stationary phase analysis of the spiral phase quadrature transform," J. Opt. Soc. Am. A **18**(8), 1871–1881 (2001).
46. Q. Kemao, "Applications of windowed Fourier fringe analysis in optical measurement: a review," Opt. Lasers Eng. **66**(3), 67–73 (2015).
47. Q. Kemao, *Windowed Fringe Pattern Analysis* (SPIE, 2013).
48. L. Huang, Q. Kemao, B. Pan, and A. K. Asundi, "Comparison of Fourier transform, windowed Fourier transform, and wavelet transform methods for phase extraction from a single fringe pattern in fringe projection profilometry," Opt. Lasers Eng. **48**(2), 141–148 (2010).
49. Z. Zhang, Z. Jing, Z. Wang, and D. Kuang, "Comparison of Fourier transform, windowed Fourier transform and wavelet transform methods for phase calculation at discontinuities in fringe projection profilometry," Opt. Lasers Eng. **50**(8), 1152–1160 (2012).
50. M. Zhao and Q. Kemao, "Multicore implementation of the windowed Fourier transform algorithms for fringe pattern analysis," Appl. Opt. **54**(3), 587–594 (2015).
51. Z. Wang and A. C. Bovik, "A universal image quality index," IEEE Signal Process. Lett. **9**(3), 81–84 (2002).
52. M. A. Herráez, D. R. Burton, M. J. Lalor, and M. A. Gdeisat, "Fast two-dimensional phase-unwrapping algorithm based on sorting by reliability following a noncontinuous path," Appl. Opt. **41**(35), 7437–7444 (2002).
53. H. Wang, C. Luo, L. Zhong, S. Ma, and X. Lu, "Phase retrieval approach based on the normalized difference maps induced by three interferograms with unknown phase shifts," Opt. Express **22**(5), 5147–5154 (2014).
54. M. Kujawińska and L. Sałbut, "Determination of mechanical joints properties by automated moiré interferometry," SPIE Proc. **3824**, 237–244 (1999).
55. K. Patorski, M. Trusiak, and T. Tkaczyk, "Optically-sectioned two-shot structured illumination microscopy with Hilbert-Huang processing," Opt. Express **22**(8), 9517–9527 (2014).
56. A. Kuś, M. Dudek, B. Kemper, M. Kujawińska, and A. Vollmer, "Tomographic phase microscopy of living three-dimensional cell cultures," J. Biomed. Opt. **19**(4), 046009 (2014).
57. K. Patorski and A. Styk, "Interferogram intensity modulation calculations using temporal phase shifting: error analysis," Opt. Eng. **45**(8), 085602 (2006).
58. L. Salbut, K. Patorski, M. Jozwik, J. Kacperski, C. Gorecki, A. Jacobelli, and T. Dean, "Active micro-elements testing by interferometry using time-average and quasi-stroboscopic techniques," Proc. SPIE **5145**, 23–32 (2003).
59. K. Patorski and M. Trusiak, "Highly contrasted Bessel fringe minima visualization for time-averaged vibration profilometry using Hilbert transform two-frame processing," Opt. Express **21**(14), 16863–16881 (2013).
60. M. Wielgus and K. Patorski, "Denoising and extracting background from fringe patterns using midpoint-based bidimensional empirical mode decomposition," Appl. Opt. **53**(10), B215–B222 (2014).

1. Introduction

Optical metrology provides contactless, full field, easily automatable and accurate means for studying diverse physical phenomena and various engineering/biological objects. Applying interferometry, structured illumination or moiré techniques one encounters measurand encoded in phase or amplitude distribution of a fringe pattern. To obtain measurand information the fringe pattern phase and/or amplitude demodulation is performed. Multiple-frame methods are considered as the most accurate ones [1–4]. Single-frame techniques are highly desired for out-of-laboratory tests enabling accurate studies of transient events in hostile environment. Among dynamically developed single frame automatic fringe pattern analysis (AFPA) techniques we have: Fourier transform [5–7], windowed Fourier transform [8–10], continuous wavelet transform [11–13], regularized phase tracking [14–16], spatial carrier phase shifting [17–22], statistical image decomposition [23,24], empirical mode decomposition aided by Hilbert transform [25–31] and monogenic signal based approach [32]. Practical challenges include certain carrier fringe applications [5–13,17–22], closed fringes analysis [5–10], error propagation [5–7,14–22] and in general susceptibility to noise, modulation/background changes and fringe form/period variations [5–24]. The most versatile and efficient solutions have very high computational load and long processing time [13,16,24]. To loosen the requirements and increase the accuracy of single-frame demodulation solutions two-frame algorithms were proposed [33–35]. The idea is to record two arbitrarily phase shifted patterns in very short time, thus no precise control nor supervision over phase shifting is necessary. Two-frame algorithms enable accurate phase demodulation regardless of considerable local fringe period and orientation changes (e.g.,

#229019 - $15.00 USD Received 8 Dec 2014; revised 26 Jan 2015; accepted 26 Jan 2015; published 13 Feb 2015

closed fringes). They often require fringe normalization [34], background removal [33,35], noise reduction [33] or phase-shift close to $\pi/2$ [34], however. Versatile approach reported in [35] is free of those requirements but it employs the minimization process severely increasing the computation burden and processing time.

Vargas et. al proposed in [36] a very fast, capable and attractive two-shot demodulation approach based on the Gram-Schmidt orthonormalization process (GS). It requires only two arbitrarily phase-shifted frames which are treated as vectors and upon orthogonal projection of one fringe vector onto another the quadrature fringe pattern pair is obtained. Its superiority both in processing time and phase demodulation accuracy over other two-shot techniques was successfully demonstrated in [36]. In this paper we recognize potential error sources and analyze their influence on the GS algorithm phase demodulation accuracy. It performs efficiently under assumption that background term is removed from fringe patterns, their modulation distribution is exactly the same in two frames and noise is suppressed. Otherwise considerable demodulation errors appear. We propose to employ fringe pattern adaptive band-pass filtering and normalization using the Hilbert-Huang transform (HHT) based approach prior to the demodulation significantly improving the GS method result and expanding its capabilities. The HHT enhanced GS approach is applied for the first time to phase demodulation of DSPI fringes. Moreover we propose to conduct the fringe pattern amplitude demodulation using the GS approach and evaluate algorithm errors proposing a solution in terms of HHT pre-filtering. Synthetic and experimental fringe pattern processing and analysis corroborates the versatility and effectiveness of the introduced HHT-GS method.

As the GS algorithm was never meant to work without preprocessing we compare the proposed technique with the GS method combined with three different pre-filtering approaches: (1) Gaussian convolution filtering for background removal and noise suppression [37] and two orthogonal band-pass filtering (TOBF) [38] for fringe normalization, (2) directional derivative (DD) algorithm [38] and (3) 2D continuous wavelet transform (CWT) method [40,41] for comprehensive fringe denoising, detrending and normalization. Throughout the paper the first mentioned reference approach is abbreviated as GS1, second as GS2 and third by CWT-GS. Therefore in total we will evaluate the performance of five different phase/amplitude demodulation approaches and show in detail that the proposed HHT-GS compares very favorably with the other ones.

The paper is constructed as follows. Section 2 describes the proposed HHT-GS methodology for its evaluation and comparison with other existing techniques. Section 3 contains results of synthetic and experimental evaluation of the proposed scheme employed for the two-shot phase demodulation. Detailed error analysis of the GS method is provided. Speckle patterns are processed and analyzed for the first time by the GS based technique. Section 4 provides results of simulations and experimental studies of the proposed HHT-GS method applied for the first time to fringe pattern amplitude demodulation. Both quantitative and qualitative evaluation results are discussed in Section 5. Section 6 concludes the paper.

2. Algorithm description

For fringe pattern band-pass filtering and normalization our approach employs the automatic selective reconstruction (ASR) algorithm described in detail in [29]. It is based on two-dimensional Hilbert-Huang transform by means of the enhanced fast empirical mode decomposition (EFEMD) and spiral Hilbert transform (HS) [29]. The one-dimensional version of the empirical mode decomposition was firstly developed in [42]. In so-called sifting process it decomposes a signal into a small number of intrinsic mode functions - meaningful oscillatory components representing signal features in different time scales. It is basis-free, adaptive and data-driven approach. The practical impact of bidimensional EMD (BEMD) is limited by extremely long irregular 2D extrema grid interpolation employed for upper and lower envelope surface generation which is the main part of the sifting process. To overcome this limitation FABEMD (Fast Adaptive BEMD) approach was proposed [43] in

#229019 - $15.00 USD Received 8 Dec 2014; revised 26 Jan 2015; accepted 26 Jan 2015; published 13 Feb 2015

which the surface interpolation is replaced by a nonlinear order-statistics-based filtering followed by a smoothing operation. Beside significantly shortening the computation time, more accurate estimation of the bidimensional intrinsic mode functions (BIMFs) representing image features at various spatial scales is obtained in many cases. Spatial frequency decreases over a set of BIMFs - first extracted BIMF contains locally highest spatial frequency component whereas the last BIMF and decomposition residue store information about low-frequency trend. Recently our group has successfully accelerated the FABEMD method using mathematical morphology for extremely fast envelope estimation. Employing so-called EFEMD algorithm [29] one can complete 512x512 pixel image decomposition under one second (Matlab implementation, medium class PC - 8 GB RAM and i7 2,1 GHz).

Modeling a fringe pattern as

$$I(x,y) = a(x,y) + b(x,y)\cos(\varphi(x,y)) + n(x,y) \tag{1}$$

where a denotes background, b is amplitude modulation, n denotes noise and φ stands for phase, one obtains high frequency noise in the first BIMFs, low frequency background in last BIMFs whereas modulated cosine term of interest is "somewhere in the middle". If the fringe pattern under study has the quasi-uniform global period (spatial frequency) then the band-pass filtered modulated cosine term can be found in a single BIMF. On the other hand if the fringe pattern has significant local period variations then the modulated cosine term of interest will spread onto couple of BIMFs making the band-pass filtering more difficult because now single BIMF will contain in some area the filtered "good fringes" and narrow-band noise in the rest of the domain. To reconstruct noise-free fringe pattern we consider, for each BIMF, only the region where sharply extracted fringes are identified. For each BIMF its amplitude distribution is calculated using the Hilbert spiral transform [44,45] and used as an indicator of the local fringe quality. High amplitude value corresponds to sharply extracted fringes. Band-pass filtered fringe pattern is obtained stitching locally identified regions with "good fringes". It is subsequently normalized by its amplitude distribution using HS. Due to its robustness to noise, modulation, background, local fringe shape, orientation and period variations the ASR approach is perfectly tailored for fringe pattern preprocessing to enhance the phase demodulation using the Gram-Schmidt orthonormalization.

Although the FABEMD/EFEMD techniques calculate adaptively the filter size used at each decomposition step (for each BIMF extraction) they employ globally the same filter size for each pixel of image during certain sifting step (upper and lower envelope surface interpolation for BIMF number n extraction). This can question the locality of our technique but it should be noted that (1) each BIMF contains locally highest spatial frequency component present in the image before this BIMF extraction and (2) the automatic selective reconstruction provides local means for analysis in terms of local fringe quality indicator application (BIMF amplitude distribution). In this form the HHT-GS robustness to local fringe direction and period variations is ensured.

Proposed preprocessing technique is compared with three schemes composed of well-established existing filtering techniques. The goal of the filtering technique is to perform fringe detrending, denoising and normalization. Each method should be a single frame technique applied to each of the two fringe patterns required by the Gram-Schmidt orthonormalization process to improve the phase calculation in case of uneven background illumination, amplitude modulation and noise. Robustness to fringe shape and period variation, as it is the inherent feature of the GS phase demodulation, should be maintained.

The first reference method abbreviated as GS1 employs Gaussian filtering for noise reduction (small window size and small standard deviation) and background rejection (large window size and large standard deviation). The window size for each filtering has to be determined manually having *a priori* knowledge of the fringe pattern under study. Once the window size is established the same amount of high frequency noise will be removed by Gaussian low-pass filtering (or low-frequency background term removed by Gaussian high-

#229019 - $15.00 USD Received 8 Dec 2014; revised 26 Jan 2015; accepted 26 Jan 2015; published 13 Feb 2015

pass filtering) globally (in each pixel neighborhood) regardless of the local fringe period. Gaussian blurring applied to remove noise or calculate the background term can introduce unwanted fringe phase variations and quality drops at image boarders. Once the noise and background is removed the normalization is performed using the two orthogonal band-pass filter method proposed by Quiroga et. al in [38]. At this point the radius of the Fourier plane mask designed to stop the DC term should be specified but since we already removed the background the radius is set to 0 (Gaussian background filtering yields better results than spectrum mask filtering). This completes the preprocessing and phase can be determined using the GS1 algorithm.

The GS2 reference algorithm employs for fringe pre-filtering the directional derivatives algorithm proposed in [39] by Ochoa et. al. This method requires manually introduced estimated fringe period value (in pixels) to ensure efficient denoising, detrending and normalization of "homogenous" fringe patterns with quasi-constant period across the domain. The larger the fringe period the more computation time is required.

Third pre-filtering (denoising, detrending and normalization) method is the 2D continuous wavelet transform (CWT) - a representative of the Fourier based techniques. It was proposed for orthonormalization pre-filtering in [41]. In this paper we use modified Mexican hat mother wavelet based algorithm [40] which is automatic, accurate and very efficient but has high computational load due to dense sampling in the wavelet coefficients domain. It is worth to note that advanced algorithm based on the notion of CWT [12, 13, 40] and Windowed Fourier Transform (WFT) [8–10,46,47] provide very similar fringe filtering, normalization and demodulation outcome [48,49], therefore CWT results presented in this paper can be linked to the WFT performance. Computation time is comparable due to recently proposed WFT multi-core implementation enabling more than a 10 fold acceleration of 1024x1024 px fringe pattern analysis [50].

3. Phase demodulation

3.1 Simulations

To show how the fringe pattern background, modulation and noise distribution affect the GS phase demodulation performance we simulated two phase-shifted by $9\pi/14$ ideal cosine terms, Figs. 1(a) and 1(b), background function, Fig. 1(c), and two different amplitude modulation functions, Figs. 1(d) and 1(e). Every image has 512x512 pixels size. Reference ideal wrapped phase map is depicted in Fig. 1(f). Synthetic pattern corrupted only with the background component is presented in Fig. 1(g), and two cosine terms with different amplitude modulation distributions are shown in Figs. 1(h) and 1(i). Synthetic fringes simultaneously spoiled with uniform random noise (randn function in Matlab), uneven background and first amplitude modulation function is presented in Fig. 1(j). Two simulated speckle fringe patterns are presented in Figs. 1(k) and 1(l). In sum the total of five cases will be considered in the simulation part, having as an input two phase shifted fringe patterns spoiled with (1) the same background function, (2) two different amplitude modulation functions, (3) background and modulation, (4) simultaneously background, modulation and noise, and (5) speckle noise. According to Eq. (1) (a - background, b - modulation, n - noise) five considered cases can be abbreviated as (1) a, (2) b, (3) a + b, (4) a + b + n, (5) speckle.

#229019 - $15.00 USD Received 8 Dec 2014; revised 26 Jan 2015; accepted 26 Jan 2015; published 13 Feb 2015

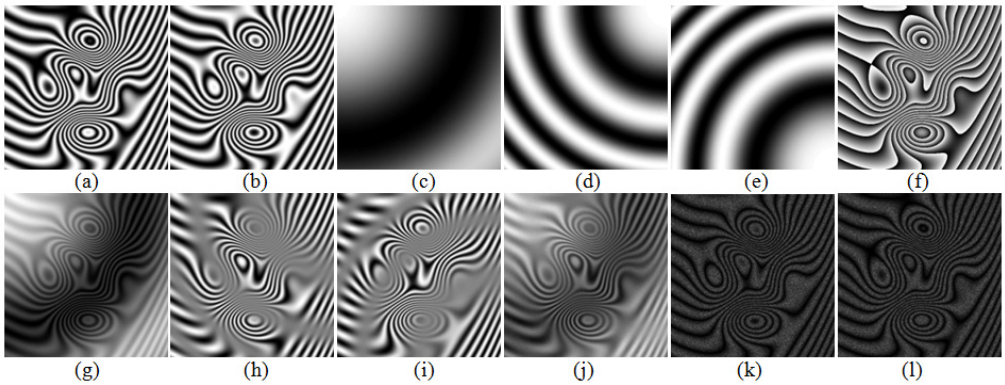

Fig. 1. Simulated cosine term (a), cosine term phase shifted by 9π/14 (b), background (c), two modulation functions (d)-(e), ideal wrapped phase (f), synthetic fringes spoiled with background (g), two phase shifted synthetic fringe patterns spoiled with different modulation functions (h)-(i), synthetic fringe pattern spoiled with modulation, background and noise (j), two synthetic speckle pattern (cosines, Figs. 1(a) and 1(b), spoiled with speckle noise) (k)-(l).

For evaluation purpose we will compare the wrapped and unwrapped phase distributions obtained under different conditions (using pure GS, GS1, GS2, CWT-GS and proposed HHT-GS algorithms) with the simulated ground truth. The image quality index proposed in [51] will be used to measure the similarity. It attains maximum value of 1 in case of identical images and adequately lower values for deteriorating demodulation efficiencies. To make the quantitative evaluation more comprehensive we calculate the RMS error values.

When applying the GS algorithm for phase demodulation of ideal cosine terms the obtained unwrapped phase map is identical with the simulated ground truth (Q = 1). If we add the same amplitude modulation distribution to our ideal cosine terms (phase shifted by 9π/14) and conduct the phase demodulation we will also end up with excellent result Q = 1. It corroborates the ability of performing efficient phase demodulation using non-normalized fringe patterns. If we consider the case when the same background term, Fig. 1(c), is added to the ideal cosine terms then we observe dramatic decrease in Q = 0.04 of demodulated unwrapped phase distribution, Fig. 2(a).

When the modulating amplitude function differs for two fringe patterns (Fig. 1(d) for first one and Fig. 1(e) for the second one) the wrapped phase distribution obtained using the GS (for two patterns, Figs. 1(h) and 1(i)) algorithm is erroneous, Fig. 2(b), exhibiting Q = 0.5. It should be noted that uneven background term is more problematic than uneven amplitude modulations, so the ability to remove the DC term in pre-filtering is of great importance in GS demodulation. Applying modulation (2 times lower than in previous example where only modulation artifacts where studied) and background defect simultaneously the obtained GS demodulated wrapped phase map, Fig. 2(c), is of very low quality (Q = 0.11) mainly due to the significant DC term variation.

When simulated white Gaussian noise is also added, Fig. 1(j), the wrapped phase map, Fig. 2(d), contains visible noise artifacts but still the most significant errors are introduced by the DC term (Figs. 2(c) and 2(d) are more similar to the Fig. 2(a) than Fig. 2(b) both in qualitative and quantitative forms). In case of two simulated speckle patterns, Figs. 1(k) and 1(l), the GS algorithm is not able to calculate meaningful wrapped phase map which could be unwrapped, Fig. 2(e). Very low Q = 0.09 indicates that speckle noise significantly deteriorates the GS phase demodulation efficiency.

Low quality of demodulated wrapped phase map directly influences the unwrapping algorithm efficiency and errors are transferred to the final AFPA result - unwrapped phase distribution. For phase unwrapping we use the algorithm proposed in [52] by Miguel Herraez et al. Unwrapped phase distributions obtained using wrapped phase maps depicted in Figs.

#229019 - $15.00 USD Received 8 Dec 2014; revised 26 Jan 2015; accepted 26 Jan 2015; published 13 Feb 2015

2(a)-2(e) attained Q values 0.07, 0.83, 0.07, 0.12 and 0.002, respectively. It should be noted that in case of very strong amplitude modulation unwrapped phase exhibited good Q = 0.83. Very low Q = 0.002 for speckle case, Fig. 2(e), can be attributed to the fact that this erroneous map simply cannot be unwrapped. Numerical evaluation results in terms of Q values calculated for different defect categories (a - background, b - modulation, n - noise, according to Eq. (1) are presented in Table 1 and Table 2 for wrapped and unwrapped phase maps, respectively. In addition the RMS error values (as a standard numerical comparison tool) were calculated and presented in Tables 3 and 4.

First part of the simulations clearly indicates strong need for efficient fringe pattern band-pass filtering and normalization prior to the GS algorithm based phase demodulation. Corresponding wrapped phase demodulation results obtained using the GS1 algorithm are presented in Figs. 2(f)-2(j). Gaussian filtering was applied for background removal (101x101 filter mask with $\sigma = 10$) and noise suppression (11x11 filter mask with $\sigma = 1.5$), and TOBF algorithm was employed for subsequent fringe normalization (radius = 0). Evaluating qualitatively and quantitatively (Q and RMS, Tables 1-4) results obtained using the GS1 algorithm one can note that it performs rather satisfactorily in case of uneven background term, amplitude modulation and white Gaussian noise ensuring dramatic increase in demodulation efficiency comparing to the standard GS algorithm. Some problems are clearly visible, however. Strong low-pass filtering for background calculation and its subsequent removal introduces artifacts on the image border, Figs. 2(f), 2(g) and 2(h). In Fig. 2(i) some residual noise can be readily recognized especially in areas with local low spatial frequency of fringes. It is due to the trade-off in low-pass filtering - larger masks blur high spatial frequency fringes whereas smaller masks leave some noise behind in areas where fringe period is large. Moreover GS1 algorithm is not robust to speckle noise, Fig. 2(j).

Algorithm proposed by Ochoa [39] (combined with GS demodulation is abbreviated in the paper as GS2) utilizes directional derivatives calculated under the assumption of quasi-constant fringe period (narrow band of spatial frequencies present in a fringe pattern). Estimated dominant fringe period has to be provided manually. Having the period value (in pixels) algorithm performs fringe pattern band-pass filtering and normalization in fully automated manner which differentiates it from the manual Gaussian filtering in GS1 scheme. Results obtained using the GS2 demodulation approach, presented in Figs. 3(a)-3(e), are similar to those calculated with GS1 algorithm in terms of Q values, Tables 1 and 2, but RMS evaluation reveals disadvantages attributed to significant local fringe period variation, Tables 3 and 4. Visual judgment also promotes the GS1 approach, but in case of speckle patterns, Fig. 3(e), GS2 exhibits better denoising in areas of quasi-constant fringe period (e.g., upper right part). Estimated fringe period of 19 pixels was set before GS2 demodulation.

In our analyses we include a representative of Fourier transform based techniques namely the 2D continuous wavelet transform (2D CWT). It provides local and accurate fringe pattern filtering due to scaling, translating and rotating a mother wavelet function (modified Mexican hat [39]) across the image in search for the highest correlation (natural band-pass filtering). It is a very powerful and automatic approach [40,41]. Results obtained using the CWT-GS approach, Figs. 3(f)-3(j), compare very favorably with the ones provided by GS1 and GS2 schemes for background removal and speckle denoising. It can be noted both in terms of visual judgment (qualitative evaluation) and Q/RMS value calculation (quantitative comparison), Tables 1-4. The CWT-GS is completely robust to uneven background term, but it can be observed that strong amplitude modulation, Fig. 3(g) top left part, imposes significant difficulties. The GS1 algorithm overcomes this limitation. With weaker fringe contrast drops algorithm operates correctly, Fig. 3(h). Both white Gaussian noise and speckle noise are transferred to the demodulated wrapped phase maps in areas where fringe period is large. It is due to the local significant difference between spatial frequency of fringe pattern and noise.

#229019 - $15.00 USD Received 8 Dec 2014; revised 26 Jan 2015; accepted 26 Jan 2015; published 13 Feb 2015

Proposed HHT-GS algorithm removes the background decomposing fringe patterns using the EFEMD technique and discarding the residue. Exemplifying decomposition results with 4 BIMFs and residue are depicted in Figs. 4(a)-4(e). The simulated uneven background term, Fig. 1(c), is extracted as the decomposition residue and can be removed for background rejection. The GS phase demodulation result, Fig. 5(a), of adaptively high-pass filtered patterns (BIMF1 + BIMF2 + BIMF3 + BIMF4) exhibits satisfactory Q = 0.71 for wrapped phase map and excellent Q = 0.98 for unwrapped phase distribution which corroborates the validity of EFEMD preprocessing. Applying the fringe pattern normalization by means of the Hilbert spiral transform prior to the GS phase demodulation enhances its efficiency, Fig. 5(b). Q increased to 0.89 and 0.99 for wrapped and unwrapped phase maps, respectively. For the case of presence of both the amplitude modulation variation and uneven background the images were first decomposed to remove the background and then adaptively high-pass filtered patterns were normalized using the Hilbert spiral transform. Preprocessing (background rejection and normalization) resulted in enhanced wrapped phase map and Q value increased to excellent value 0.97 (calculated after unwrapping).

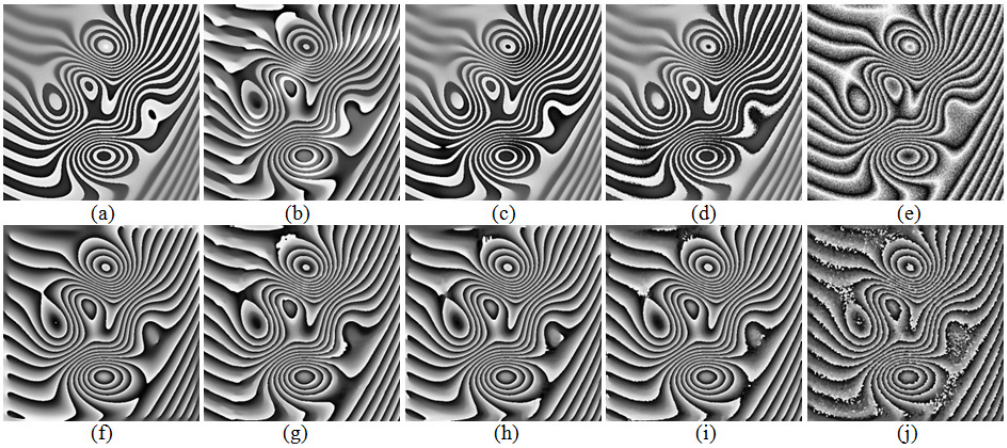

Fig. 2. Wrapped phase maps obtained using the GS algorithm applied to synthetic patterns spoiled with background (a), modulation (b), modulation and background (c), modulation, background and noise (d), and speckle noise (e); corresponding wrapped phases obtained using the GS1 algorithm (f)-(j).

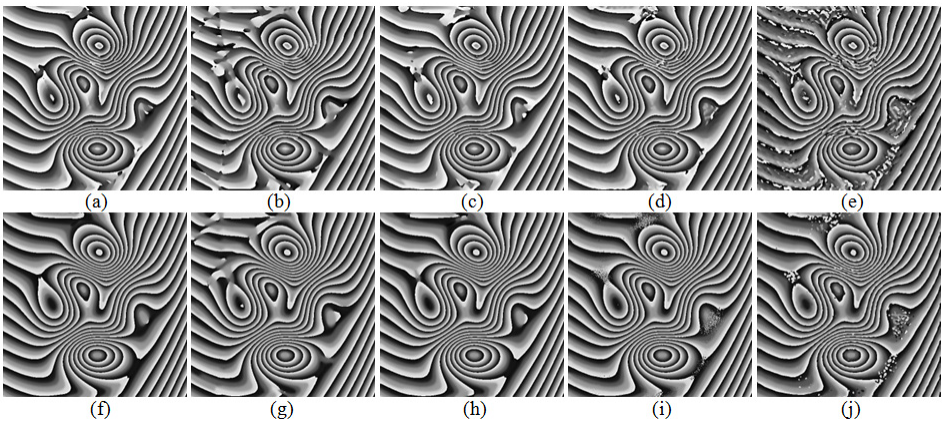

Fig. 3. Wrapped phase maps obtained using the GS2 algorithm applied to synthetic patterns spoiled with background (a), modulation (b), modulation and background (c), modulation, background and noise (d), and speckle noise (e); corresponding wrapped phases obtained using the CWT-GS algorithm (f)-(j).

#229019 - $15.00 USD Received 8 Dec 2014; revised 26 Jan 2015; accepted 26 Jan 2015; published 13 Feb 2015

White Gaussian noise of variance 0.005 added to the ideal cosine terms alongside with modulation and background caused more sophisticated filtering scheme to be employed. Automatic selective reconstruction algorithm [29] is especially tailored for filtering out the noise and background and performing the fringe pattern normalization. The ASR was applied for adaptive denoising, detrending and normalization of two synthetic patterns significantly increasing the GS phase demodulation efficiency, Fig. 5(d), reaching Q = 0.97 (after unwrapping). When fringe patterns are spoiled with speckle noise the strategy remains the same. The ASR algorithm decomposes the speckle pattern - exemplifying decomposition results are presented in Figs. 4(f)-4(o) - and considers for reconstruction only specific areas of each BIMF where sharply extracted fringes are encountered. Demodulated wrapped phase map is depicted in Fig. 5(e). Proposed HHT-GS approach attains the highest Q values (0.69 and 0.96 for wrapped and unwrapped case, respectively) and lowest RMS errors (1.12 and 0.34 for wrapped and unwrapped case, respectively) from all of the tested pre-filtering techniques. It is worth to note that the ASR approach is the unique one ensuring high efficiency denoising in troublesome areas where fringe period is large.

Taking closer look at the four Tables containing the numerical evaluation results one can readily notice that HHT-GS technique ensures the best demodulation quality both in terms of the Q and RMS values calculated for wrapped and unwrapped phase maps. The unwrapped phase distribution evaluation is of main importance since it is the final result of the automatic fringe pattern processing but in this paper wrapped phase maps were presented as they constitute the result of the GS demodulation. Calculated Q and RMS values, Tables 1-4, corroborate the validity of the HHT-GS approach and promote it over other pre-filtering schemes. Presented numerical studies verify that HHT-GS exhibits robustness to uneven background term, strong amplitude modulation, white Gaussian noise and speckle noise, fringe pattern local period and orientation variations.

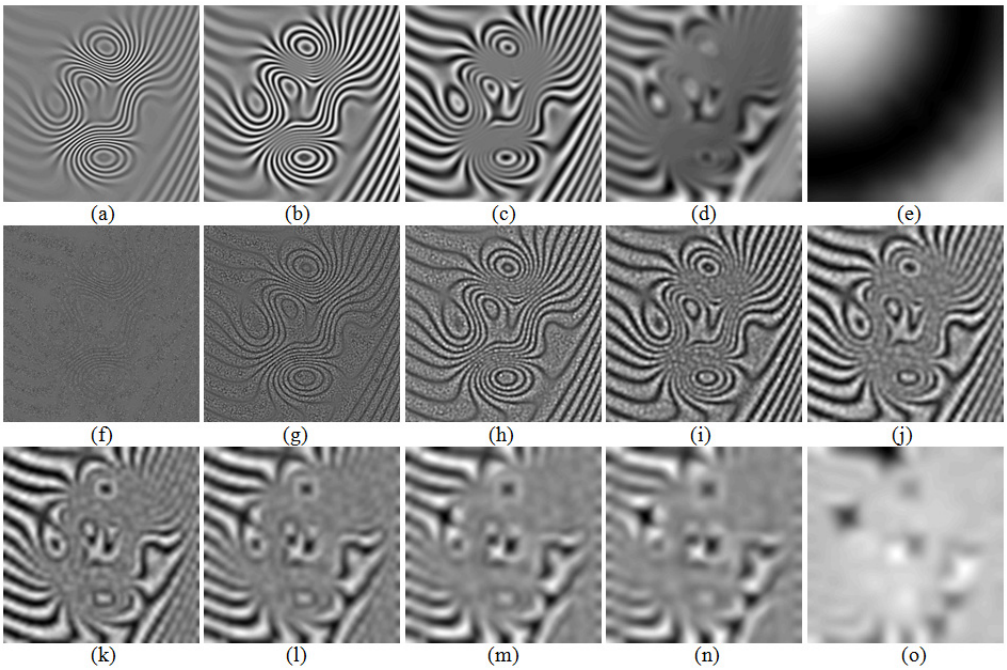

Fig. 4. (a)-(e) First four BIMFs and the residue obtained decomposing the synthetic pattern with background, Fig. 1(g), using the EFEMD algorithm; (f)-(o) first nine BIMFs and the residue obtained decomposing the synthetic speckle pattern, Fig. 1(k), using the accelerated FABEMD algorithm.

#229019 - $15.00 USD Received 8 Dec 2014; revised 26 Jan 2015; accepted 26 Jan 2015; published 13 Feb 2015

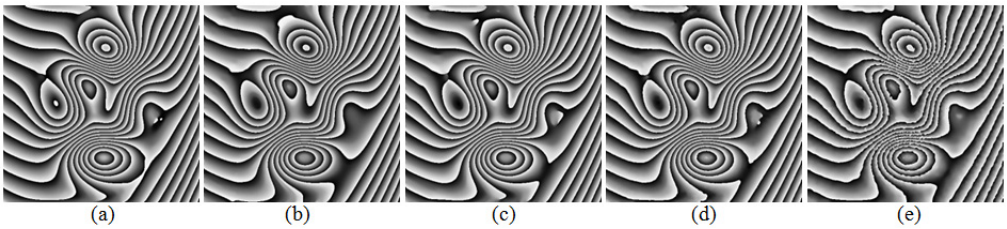

Fig. 5. Wrapped phase maps obtained using the HHT-GS algorithm applied to synthetic patterns spoiled with background (a), modulation (b), modulation and background (c), modulation, background and noise (d), and speckle noise (e).

To conclude numerical studies the calculation time evaluation for each method and each simulated case is presented in Table 5 (b - just modulation variation, a - just background illumination, n - just noise added). Regular GS algorithm with no pre-filtering is extremely fast operating in 0,09s for 512x512 pixel images (Matlab implementation, medium class PC - 8 GB RAM and i7 2,1 GHz). The GS1 algorithm is very fast due to well-optimized Gaussian filtering (around 0.04s per image per operation) and Fourier transform based TOBF normalization (around 0.1s per image). It total calculations last around 0.5s but *a priori* knowledge on appropriate filter size and standard deviation is required. Manually converging to the best filtering parameters may take around a minute. The computational load of the GS2 algorithm is determined by the estimated fringe spacing - the larger it is the longer the calculations. In our case it was around 45s per image yielding more than 90s in total for demodulation. Longer computation time is leveled by the automatic operation. The 2D-CWT automatic filtering requires 14s for each of two fringe images under study.

Table 1. Wrapped phase demodulation quality evaluation (Q values)

	a	b	a + b	a + b + n	speckle
GS	0.04	0.5	0.11	0.13	0.09
GS1	0.63	0.76	0.75	0.76	0.45
GS2	0.69	0.58	0.65	0.69	0.45
CWT-GS	0.72	0.63	0.7	0.67	0.62
HHT-GS	0.71	0.89	0.83	0.81	0.69

Table 2. Unwrapped phase demodulation quality evaluation (Q values)

	a	b	a + b	a + b + n	speckle
GS	0.07	0.83	0.07	0.12	0.002
GS1	0.93	0.95	0.92	0.93	0.75
GS2	0.93	0.84	0.91	0.92	0.73
CWT-GS	0.94	0.88	0.93	0.91	0.91
HHT-GS	0.98	0.99	0.97	0.97	0.96

Table 3. Wrapped phase demodulation quality evaluation (RMS values in radians)

	a	b	a + b	a + b + n	speckle
GS	3.19	1.51	3.26	3.3	2.2
GS1	1.27	0.98	1.06	0.98	2.5
GS2	1.25	1.5	1.37	1.21	1.74
CWT-GS	0.99	1.22	1.02	1.07	1.3
HHT-GS	1.01	0.69	0.83	0.84	1.12

Calculation time of the proposed HHT pre-filtering depends on the type of the operation. The more complicated our two fringe patterns are the more time we need to enhance the GS outcome. For single fringe pattern normalization the Hilbert transform algorithm needs around 0.1s, for background rejection EFEMD algorithm needs approx. 1s, and for adaptive denoising the ASR algorithm needs up to 4.5s. In total for automatic two image HHT-based

#229019 - $15.00 USD Received 8 Dec 2014; revised 26 Jan 2015; accepted 26 Jan 2015; published 13 Feb 2015

enhancement and GS demodulation we need approx. 9 seconds as indicated in Table 5. Although it is 18 times longer than for GS1 approach it is current state-of-the-art for 2D empirical mode decomposition analysis. As it was proven in this Section automatic HHT-GS provides better results than manual Gaussian filtering, which is very fast under the assumption that kernel size and standard deviation are known *a priori*.

Table 4. Unwrapped phase demodulation quality evaluation (RMS values in radians)

	a	b	a + b	a + b + n	speckle
GS	54.99	0.7	61.3	60.9	69.5
GS1	1.71	0.39	0.64	0.62	1.64
GS2	2.25	2.46	2.19	1.88	2.23
CWT-GS	0.27	0.89	0.33	0.68	0.45
HHT-GS	0.26	0.19	0.33	0.28	0.34

Table 5. Computation time assessment (seconds)

	a	b	a + b	a + b + n	speckle
GS	0.09	0.09	0.09	0.09	0.09
GS1	0.17	0.37	0.46	0.52	0.51
GS2	92.1	90.2	91.2	96.3	98.2
CWT-GS	28.5	28.4	29.1	29.4	29.6
HHT-GS	2.19	0.21	2.2	8.91	9.08

It is worth to emphasize that Gram-Schmidt orthonormalization process produces erroneous results when two fringe patterns (treated as vectors) are out-of-phase (phase-shifted exactly by π) or identical (phase shifted exactly by 0) [53]. Considering vectors it corresponds to cases of two parallel (linearly dependent) vectors or identical vectors. Pre-filtering techniques applied to two out-of-phase fringe patterns prior to the demodulation are not able to suppress the GS process errors. This limitation can be avoided using three frame approach [53] and calculating two normalized difference maps (as an input to the GS process). In [53] influence of phase-shift on the two and three frame GS process was studied and is not to be repeated herein. It is worth to note that approach proposed in [53] uses third frame not only to avoid the π -phase-shift limitation but also to remove background term upon subtraction. In our scheme background term is quickly and very efficiently eliminated using the EFEMD decomposition - third frame is not needed (which may be troublesome to record with the same background term like two previous frames; background has to be identical in each frame to enable its elimination upon subtraction).

3.2. Experiments

For experimental corroboration real fringe patterns obtained by grating interferometry (GI) [54], Fig. 6(a) and 6(b) and Fig. 7(a) and 7(b), and digital speckle pattern interferometry (DSPI), Fig. 8(a) and 8(b), were used.

The GI setup was assembled to test the stress release by cutting the metal-ceramic joint. Fringes correspond to displacement distribution, u and v in x and y directions (Figs. 6 and 7, respectively). The fringes obtained show relatively strong influence of speckles due to rough surface of the object grating. Speckles additionally complicate the analysis. For quantitative evaluation of phase demodulation quality we need to establish a reference technique. 4-frame temporal phase shifting technique serves this purpose very well. We decided to apply 3x3 Gaussian low-pass filtering (standard deviation 0.5) on each frame prior to TPS phase demodulation to reduce the influence of speckles.

In case of u displacement fringes two patterns phase shifted by $\pi/2$, Figs. 6(a) and 6(b), were phase demodulated using the regular GS algorithm yielding erroneous phase map, Fig. 6(c). Reference wrapped phase map obtained using TPS without and with Gaussian filtering are presented in Figs. 6(d) and 6(e), respectively. The GS1 algorithm outcome is depicted in

#229019 - $15.00 USD Received 8 Dec 2014; revised 26 Jan 2015; accepted 26 Jan 2015; published 13 Feb 2015

Fig. 6(f) - residual noise and demodulation artifacts can be readily noted especially in areas with sparse fringes and at the image borders (top and bottom). The GS2 algorithm deteriorates where fringe spacing is significantly bigger than estimated one, Fig. 6(g). The CWT-GS approach is able to provide very smooth phase fringes in full field, Fig. 6(h). Comparing to the reference filtered-TPS outcome the 2D-CWT produces over-smoothed patterns therefore significantly smoothed phase distribution - fine information is lost. The proposed HHT-GS algorithm with ASR filtering and normalization shows excellent robustness to noise and fringe density variations providing detailed wrapped phase map, Fig. 6(i), which vividly resembles the reference, Fig. 6(e), and prevents the oversmoothing.

Results obtained in the case of *v* displacement field fringes are presented in Fig. 7 in corresponding manner. Tables 6 and 7 contain quantitative evaluation in terms of RMS error and Q values calculated for wrapped (W) and unwrapped (U) phase distributions considering the filtered TPS outcome, Fig. 6(e) and Fig. 7(e), as a reference. The HHT-GS and CWT-GS methods show the best performance. However, the oversmoothing is encountered in the CWT-GS outcome.

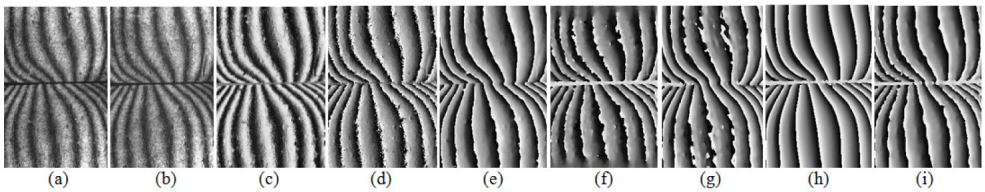

Fig. 6. Two phase-shifted real *u(x,y)* fringe patterns recorded using the grating interferometry method (a)-(b), wrapped phases obtained using the GS algorithm (c), 4-frame temporal phase shifting method (d), Gaussian filtered TPS (e), GS1 (f), GS2 (g), CWT-GS (h) and HHT-GS (i) algorithms.

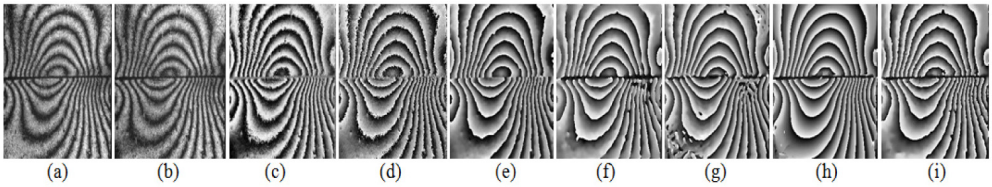

Fig. 7. Two phase-shifted real *v(x,y)* fringe patterns recorded using the grating interferometry method (a)-(b), wrapped phases obtained using the GS algorithm (c), 4-frame temporal phase shifting method (d), Gaussian filtered TPS (e), GS1 (f), GS2 (g), CWT-GS (h) and HHT-GS (i) algorithms.

Table 6. Experimental phase demodulation quality evaluation (RMS values in radians) - *u(x,y)*

	RMS W	RMS U	Q W	Q U
GS	18.05	19.8	0.10	0.09
GS1	1.41	2.78	0.52	0.76
GS2	1.31	0.58	0.52	0.83
CWT-GS	1.21	0.43	0.53	0.92
HHT-GS	1.22	0.38	0.60	0.93

Real fringe patterns presented in Figs. 8(a) and 8(b) were obtained in DSPI studies of plate bending. The approximate phase shift is equal to $\pi/2$. The GS algorithm without pre-filtering calculates very noisy phase map, Fig. 8(c). Applying GS1, GS2 or CWT-GS schemes more adequate wrapped phase maps can be determined, Figs. 8(d)-8(f). Some artifacts attributed to the speckle noise are clearly observable, however. In case of the proposed HHT-GS

#229019 - $15.00 USD Received 8 Dec 2014; revised 26 Jan 2015; accepted 26 Jan 2015; published 13 Feb 2015

processing and analysis smooth wrapped phase map is calculated, Fig. 8(g). Presented results demonstrate the GS robustness to speckle noise gained by pre-filtering.

Table 7. Experimental phase demodulation quality evaluation (RMS values in radians) - *v(x,y)*

	RMS W	RMS U	Q W	Q U
GS	18.35	20.5	0.11	0.10
GS1	1.29	2.58	0.31	0.88
GS2	1.27	0.48	0.35	0.89
CWT-GS	1.15	0.44	0.41	0.92
HHT-GS	1.19	0.38	0.37	0.93

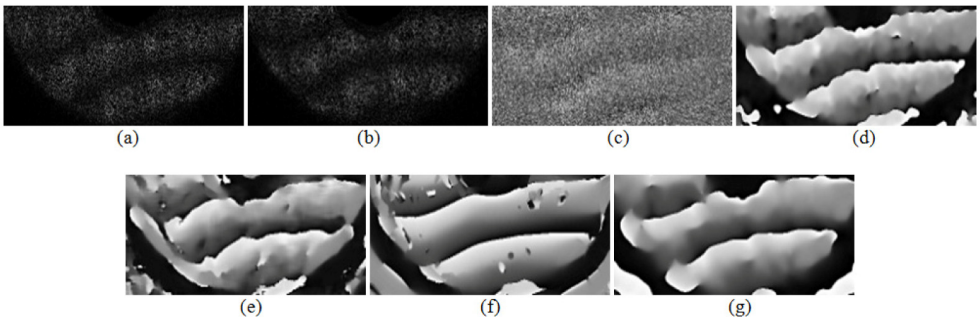

Fig. 8. Two frames of real DSPI fringes (a-b), wrapped phase demodulated using the GS (c), GS1 (d), GS2 (e) CWT-GS (f), HHT-GS (g).

It should be noted that without pre-filtering the wrapped phase map is of no physical meaning, whereas the TPS method is noise sensitive. Proposed HHT based preprocessing expands the GS algorithm onto a particularly cumbersome DSPI field; this feature is considered as one of the main novelties of the paper. Due to low quality and small number of DSPI experimental frames recorded establishing a reference phase demodulation method to provide quantitative evaluation was troublesome. Qualitative evaluation using visual judgment (Fig. 8) can confirm, however, findings presented and proved in numerical subsection 3.1.

4. Amplitude demodulation

The GS algorithm is essentially very similar to the Hilbert transform - using orthogonal projection it produces a quadrature component of a signal under study. Having two fringe patterns in quadrature we can readily obtain phase demodulation applying the arc tangent function. This was firstly noticed and described in [36]. Obtaining the fringe pattern phase distribution is of main interest in majority of cases but sometimes we stumble upon an optical measurement with measurand encoded not in the fringe phase but in its amplitude distribution. Time-averaged interferometry (TAI), moiré techniques, structured illumination microscopy [55] and tomographic phase microscopy [56] can serve as examples. In this paper we expand the GS regime to amplitude encoded fringe patterns. We demonstrate that pre-filtering in terms of Hilbert-Huang transform enhances the amplitude demodulation quality. Proposed HHT-GS approach compares favorably with Gaussian filtering.

In this Section we are interested in amplitude distribution demodulation therefore fringe normalization is not needed. For pre-processing we apply band bass filtering for noise suppression and background rejection in terms of HHT and Gaussian kernels. Automatic selective reconstruction algorithm is used without the normalization step.

#229019 - $15.00 USD Received 8 Dec 2014; revised 26 Jan 2015; accepted 26 Jan 2015; published 13 Feb 2015

4.1. Simulations

We propose to use the HHT-GS algorithm for efficient fringe pattern amplitude demodulation. HHT filtering is extremely important - GS amplitude demodulation errors are similar to those exhibited for phase demodulation. To quantitatively evaluate its performance we simulated cosine carrier fringes, Fig. 9(a), and first kind zero order Bessel modulation function, Fig. 9(b). Those two components multiplicatively superimposed create synthetic amplitude modulated fringe pattern, Fig. 9(c). Second synthetic pattern required by the GS algorithm was obtained in a similar manner by shifting carrier pattern by $\pi/7$. Ideal demodulated amplitude, Fig. 9(d), constitutes an absolute value of the simulated Bessel function, Fig. 9(b). It is used as a reference for Q value and RMS error calculations.

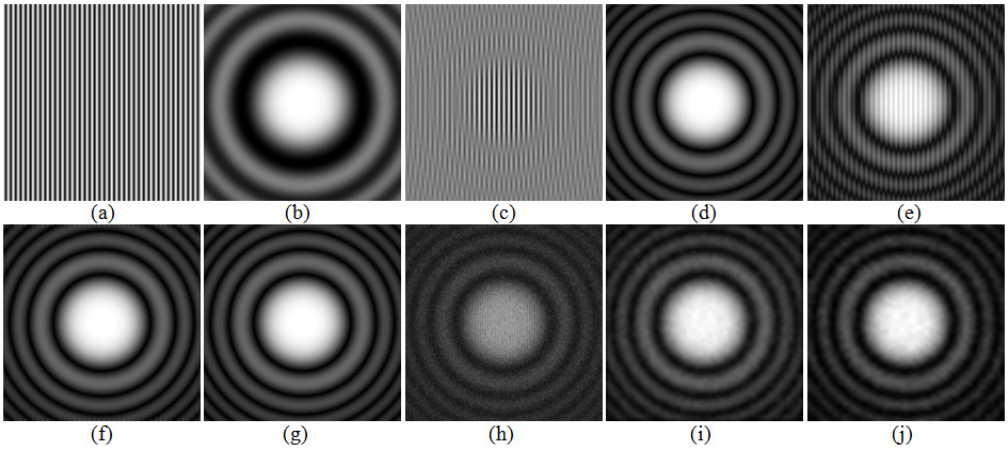

Fig. 9. Simulated cosine carrier pattern (a), Bessel amplitude modulation function (b), synthetic fringe pattern with carrier term modulated by amplitude function (c), the ideal modulus of the modulation function (d), amplitude distribution demodulated using the GS (e), GS1 (f) and the HHT-GS algorithm (g) in case of non-zero DC term; amplitude distribution demodulated using the GS (h), GS1 (i) and the HHT-GS (j) algorithm in case of noise presence.

When we employ the GS algorithm for the amplitude demodulation of synthetic patterns we obtain result very similar to the ideal case, Fig. 9(b), with Q = 0.999. This is due to the fact that simulated pattern have no background term (DC = 0). When we set DC equal to 0.1 the erroneous amplitude with strong influence of parasitic fringes [57], Fig. 9(e), is calculated using the GS algorithm, Q = 0.22. Applying the EFEMD based background removal significantly increased amplitude demodulation quality, Fig. 9(f), Q = 0.99. Gaussian high pass filtering for background suppression is also very effective increasing the Q value to 0.97. Calculated RMS errors promote the HHT-GS approach, however. Numerical evaluation results are presented in Table 8. It should be noted that EFEMD decomposition provides adaptive and straightforward means for DC term removal whereas the size and standard deviation of Gaussian kernel have to be determined manually.

If two component fringe patterns are spoiled with noise, a considerable decrease in amplitude demodulation follows, Fig. 9(h), with Q = 0.06. Employing adaptive HHT based denoising we were able to reduce the noise influence on demodulated amplitude distribution, Fig. 9(i), and increase the value of Q to 0.73. Low pass Gaussian filtering also ensures satisfactory results, Fig. 9(j), in terms of Q value but demonstrates higher RMS error. In case of simultaneous presence of both nonzero DC and noise two techniques (Gaussian and HHT based band-pass filtering) exhibit similar performance, Table 8.

Presented numerical results corroborate HHT-GS robustness to noise and uneven background when amplitude demodulation is of interest. Gaussian filtering also provides good results - its advantage is very short calculation time (around 0.2 seconds comparing to 2

#229019 - $15.00 USD Received 8 Dec 2014; revised 26 Jan 2015; accepted 26 Jan 2015; published 13 Feb 2015

seconds of HHT based processing) but kernel size and standard deviation has to be determined manually prior to the analysis.

Table 8. Amplitude demodulation quality evaluation (Q values/RMS values in radians)

	a	n	a + n
GS	0.22/0.067	0.06/0.164	0.04/0.17
GS1	0.97/0.007	0.72/0.069	0.73/0.37
HHT-GS	0.99/0.001	0.73/0.046	0.74/0.36

4.2. Experiments

Experimental evaluation is conducted using real fringe patterns obtained in TAI silicon membrane vibration testing [58]. Exemplifying two raw interferograms phase shifted by π/2 are presented in Figs. 10(a) and 10(b). In [59] we proposed very efficient two-frame technique (two π phase shifted frames subtracted) which utilizes the FABEMD decomposition and Hilbert spiral transform for amplitude demodulation. The reference FABEMD-HS result is depicted in Fig. 10(c). Applying the GS algorithm erroneous amplitude distribution is obtained, Fig. 10(d). Note low dynamic range and strong influence of parasitic fringes [57]. Two component frames EFEMD-based background removal prior to the GS amplitude demodulation resulted in significant improvement, Fig. 10(e). Gaussian high pass pre-filtering exhibits similar result, Fig. 10(f). To further increase the processing quality we employed a similar approach as in [52] - two frames required for GS demodulation (fr1, fr2) were obtained upon subtraction of two π phase shifted raw frames (fr1 = raw[0] - raw[π]; fr2 = raw[π/2] - raw[3π/2], raw[0] and raw[π/2] presented in Figs. 10(a) and 10(b)). Figure 10(g) depicts the resulting GS outcome - dynamic range has increased whereas parasitic modulation fringes are still present. They can be efficiently removed employing fr1 and fr2 background removal using the EFEMD decomposition, Fig. 10(h), or Gaussian high pass filtering, Fig. 10(i). Numerical evaluation in terms of Q value and RMS error calculation is presented in Table 9. Basing on the obtained results we advocate the use of HHT-GS algorithm for analysis of amplitude encoded fringe patterns.

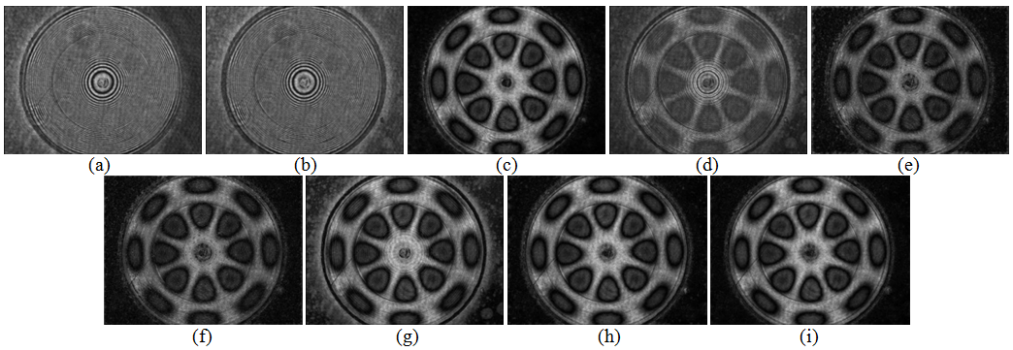

Fig. 10. Two experimental TAI frames (a)-(b), amplitude demodulation using the two-frame reference algorithm [59] (c), 2-frame GS method (d), 2-frame GS1 (e), 2-frame HHT-GS (f) and modified 4-frame GS (g), GS1 (h) and HHT-GS (i) approach.

To demonstrate the improvement made employing the HHT based pre-filtering we calculated amplitude demodulation error maps computed upon subtracting from the reference Bessel fringes (obtained using the 2-frame technique proposed in [59], Fig. 10(c)) the ones determined using the 2-frame GS, Fig. 10(d), 2-frame HHT-GS, Fig. 10(d), 4-frame GS, Fig. 10(g) and 4-frame HHT-GS, Fig. 10(h). Error maps are presented in Fig. 11. Parasitic modulation fringes removal can be readily noted comparing results obtained before and after background rejection (Fig. 11(a) with Fig. 11(b) and Fig. 11(c) with Fig. 11(d)). Enhancement

#229019 - $15.00 USD Received 8 Dec 2014; revised 26 Jan 2015; accepted 26 Jan 2015; published 13 Feb 2015

in terms of dynamic range introduced by the 4-frame GS method over the 2-frame one is readily observable (comparing Fig. 11(a) with Fig. 11(c) and Fig. 11(b) with Fig. 11(d)).

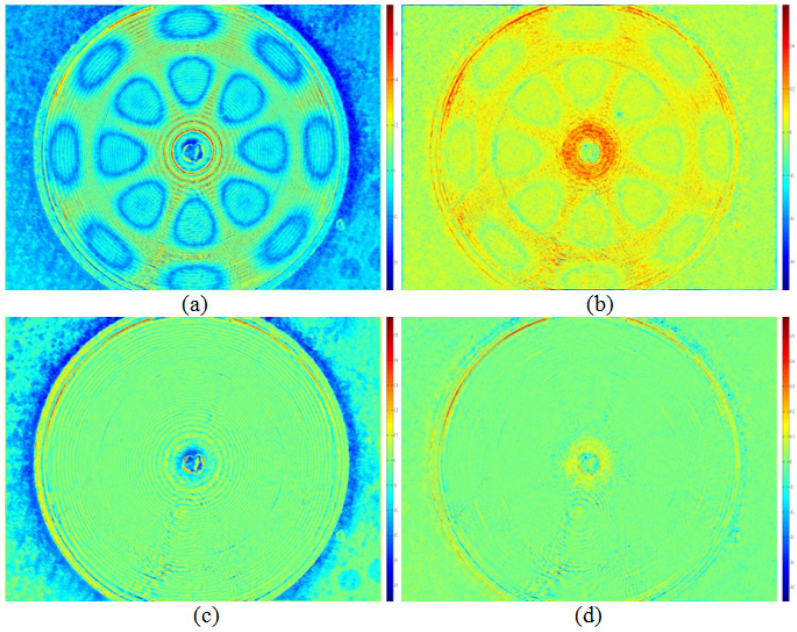

Fig. 11. Amplitude demodulation error computed upon subtracting from the reference Bessel fringes obtained using the 2-frame technique proposed in [59], Fig. 10(c), the results of (a) 2-frame GS Fig. 10(d), (b) 2-frame HHT-GS, Fig. 10(d), (c) 4-frame GS, Fig. 10(g) and (d) 4-frame HHT-GS, Fig. 10(h).

Table 9. Experimental amplitude demodulation evaluation (Q values/RMS values in radians)

	2-frame	4-frame
GS	0.18/0.156	0.39/0.115
GS1	0.35/0.095	0.65/0.046
HHT-GS	0.37/0.086	0.66/0.045

5. Discussion

Main advantage of the proposed HHT-GS algorithm over other pre-filtering techniques is that it is fully automatic, adaptive and very efficient. Employing the automatic selective reconstruction even very complicated pattern can be enhanced in 4.5 seconds. In simpler cases if we have *a priori* knowledge of the fringe pattern and kind of operation we want to perform (e.g., single spatial frequency fringes with background to be removed) we can shorten the computation time fixing the number of BIMFs to be extracted and removed (e.g., we calculate first 3 BIMFs and stop the decomposition considering the rest as a background). In this way we can increase the calculation speed and finish computing under 1 second (e.g., 512x512 pattern with background, Fig. 1(g), can be high-pass filtered keeping first three BIMFs in 0.6s). It is still more than Gaussian filtering requires but current implementation of the EFEMD decomposition is state-of-the-art in terms of computation time (for single core calculations). It will be further accelerated utilizing parallel computing architecture (like CUDA or FPGA) and calculation time similar to Gaussian filtering is expected to be reached. Gaussian filtering is very well-optimized in Matlab environment enabling extremely short calculation times.

The HHT processing is performed adaptively and there is no need to find the best kernel size and standard deviation. It is hard to determine whether the result obtained using Gaussian

#229019 - $15.00 USD Received 8 Dec 2014; revised 26 Jan 2015; accepted 26 Jan 2015; published 13 Feb 2015

filters with certain manually defined parameters is the best one possible. Searching for the right set of parameters can be time consuming and has to be performed for each image separately. Moreover utilizing HHT one obtains more accurate demodulation result and does not encounter considerable quality deterioration at image borders.

In the ASR algorithm we need more BIMFs to provide better selectivity ensuring more efficient denoising. The EFEMD algorithm utilizes relatively large filters therefore has low "modal sensitivity" - only a few BIMFs are calculated. For the purpose of increasing the number of BIMFs and enhancing the ASR outcome the accelerated FABEMD technique can be used for decomposition (it is regular FABEMD algorithm OSFW 2 [43] accelerated by morphological envelope estimation [29]). Another choice is to apply the midpoint-based bidimensional empirical mode decomposition providing more decomposition elements and better ability to separate distinct components [60]. It would be interesting to compare the performance of nonlinear EFEMD decomposition with space-scale linear iterative Gaussian high-pass filtering using kernel size determination like in EFEMD algorithm (based on extrema map characteristic). We are currently focusing on this issue and separate paper will be devoted to this issue.

In general results obtained using the CWT-GS approach are similar to the HHT-GS case (slightly lower Q and higher RMS values). 2D CWT processing is automatic, accurate and local approach ensures correct analysis even for significant local variation of fringe period, orientation and shape. In case of sparse fringes, however, errors are encountered. Accurate algorithms exhibit high computational load due to large number of wavelet coefficients to be determined. For complicated 512x512 image (i.e., Fig. 1(k)) it takes approximately 3 times longer to finish 2D CWT enhancement than the HHT based one. For simpler patterns the ratio is greater.

Presented detailed numerical and experimental studies showed that with appropriate filtering very accurate phase and amplitude demodulation can be performed using the Gram-Schmidt orthonormalization method even for demanding speckle patterns. It is very capable and fast algorithm enabling efficient analysis of fringe patterns with considerable local fringe shape, orientation and period variation. No precise control of the phase-shift between two component images is required which makes this technique very fast, robust to environmental disturbances and loosens the setup hardware requirements.

6. Conclusions

In this contribution we performed error analysis of the Gram-Schmidt orthonormalization method for fringe pattern phase demodulation. The influence of uneven background term, variable amplitude modulation and noise (white Gaussian and speckle) was studied and strong need for image pre-filtering was concluded. The Hilbert-Huang transform based automatic and adaptive pre-filtering including: (1) background removal, (2) noise reduction and (3) normalization was proposed to enhance the efficiency of Gram-Schmidt orthonormalization method applied to two-frame fringe pattern phase demodulation. The HHT method was compared qualitatively and quantitatively with other fringe filtering techniques both in terms of numerical simulations and real fringe pattern processing. It outperforms other pre-filtering techniques showing excellent robustness to noise, uneven background term, local fringe contrast drops, orientation/period variations and speckles. The GS algorithm aided with the HHT method was applied for the first time for phase demodulation of DSPI fringes and amplitude demodulation of amplitude encoded fringe patterns. Amplitude demodulation efficiency was enhanced by the HHT based denoising and background rejection. The GS amplitude demodulation error analysis and quantitative evaluation of HHT-GS approach were provided.

Numerical and experimental results corroborate the validity, robustness and versatility of the proposed HHT-GS technique both in terms of phase and amplitude demodulation of highly defected fringe patterns with significant fringe shape variation (i.e. closed fringes).

#229019 - $15.00 USD Received 8 Dec 2014; revised 26 Jan 2015; accepted 26 Jan 2015; published 13 Feb 2015

Appropriate pre-filtering enables to take full advantage of excellent features of the Gram-Schmidt orthonormalization method.

Acknowledgments

This work was supported, in part, by Ministry of Science and Higher Education budget funds for science in the years 2012-2015 as a research project in the "Diamond Grant" programme, partly by National Science Center, Poland, under the project DEC-2012/07/B/ST7/01392, in part by statutory funds and grant founded by the Dean of Faculty of Mechatronics, Warsaw University of Technology (WUT). Work of MT was partially supported by the European Union (EU) in the framework of European Social Fund through the WUT Development Programme and Foundation for Polish Science. The experimental work described in [58], from which some data were taken, was co-supported by the European Union (EU) Project OCMMM (a part of the experiments under this project was performed at Laboratoire d'Optique P.M. Duffieux, Université de Franche-Comté, Besancon, France). Authors would like to thank L. Salbut and A. Kus for providing experimental data.

#229019 - $15.00 USD Received 8 Dec 2014; revised 26 Jan 2015; accepted 26 Jan 2015; published 13 Feb 2015